

Evolution of optical properties of chromium spinels CdCr_2O_4 , HgCr_2S_4 , and ZnCr_2Se_4 under high pressure

K. Rabia¹, L. Baldassarre¹, J. Deisenhofer², V. Tsurkan^{2,3}, and C. A. Kuntscher^{1*}

¹ *Experimentalphysik II, Universität Augsburg, Universitätstr. 1, 86159 Augsburg, Germany*

² *Experimentalphysik V, Universität Augsburg, Universitätstr. 1, 86159 Augsburg, Germany and*

³ *Institute of Applied Physics, Academy of Sciences of Moldova, MD2028 Chisinau, R. Moldova*

(Dated: May 20, 2021)

We report pressure-dependent reflection and transmission measurements on ZnCr_2Se_4 , HgCr_2S_4 , and CdCr_2O_4 single crystals at room temperature over a broad spectral range 200-24000 cm^{-1} . The pressure dependence of the phonon modes and the high-frequency electronic excitations indicates that all three compounds undergo a pressure-induced structural phase transition with the critical pressure 15 GPa, 12 GPa, and 10 GPa for CdCr_2O_4 , HgCr_2S_4 , and ZnCr_2Se_4 , respectively. The eigenfrequencies of the electronic transitions are very close to the expected values for chromium crystal-field transitions. In the case of the chalcogenides pressure induces a red shift of the electronic excitation which indicates a strong hybridization of the Cr d-bands with the chalcogenide bands.

PACS numbers: 61.50.Ks,61.50.Ks,64.70.K-

I. INTRODUCTION

Chromium spinel compounds with formula $A\text{Cr}_2X_4$, where A is a divalent non-magnetic cation and X a divalent anion, exhibit many interesting phenomena such as strong geometric frustration,¹⁻³ relaxor multiferroicity,⁴ or three-dimensional topological effects.⁵ At room temperature these spinels are cubic (space group $\text{Fd}\bar{3}\text{m}$), where the non-magnetic A-site ions are tetrahedrally coordinated and the Cr^{3+} ions (electronic configuration $3d^3$ with spin $S = 3/2$) in octahedral environment form a pyrochlore lattice (see Fig. 1).

The inherent frustration of the pyrochlore lattice is often released by magneto-elastic interactions such as the spin-driven Jahn-Teller effect,^{6,7} which lead to a reduced structural symmetry coinciding with the onset of long-range magnetic order. The magneto-structural phase transition is reflected in the splitting of infrared (IR) and Raman active phonons and the crystal-field (CF) excitations, which are sensitive to changes of the magnetic and the crystalline symmetry.^{1,8-11} Since magnetic interactions depend on interatomic distances,³ one can expect structural anomalies not only at low temperatures but also at high pressures.

In general, the application of pressure can be used to tune in a controlled fashion the electronic and structural properties of a system, while optical spectroscopy is a powerful method to investigate the electronic and vibrational properties of a material. The combination of the two techniques thus allows to follow the evolution of the phonon frequencies and the (possible) splitting of optical phonon modes with applied pressure, providing useful information on both the magnetic^{9,12,13} and structural properties. The far-infrared studies on the spinel compounds can indeed reveal information on the structural properties (e.g., cation ordering, bond strengths and ionicities), on the free carrier contribution, and on magnetic phenomena.¹⁴

Earlier work on the pressure effects in chromium

spinel has concentrated on alterations of the crystal structure.^{3,15} In this work we focus on the effect of pressure on the optical properties of ZnCr_2Se_4 , HgCr_2S_4 , and CdCr_2O_4 spinels in a broad frequency range (200-24000 cm^{-1}) at room temperature. Based on the pressure dependence of the phonon modes and the electronic excitations we propose the occurrence of a pressure-induced structural phase transition in all three compounds.

The paper is organized as follows: In Section I we discuss the experimental details of the pressure measurements and the data analysis procedure. We present the obtained optical spectra in Section II, discuss the results in Section III, and summarize our findings in Section IV.

II. EXPERIMENT

We have investigated the three single-crystalline Cr-spinels ZnCr_2Se_4 , HgCr_2S_4 , and CdCr_2O_4 by means of

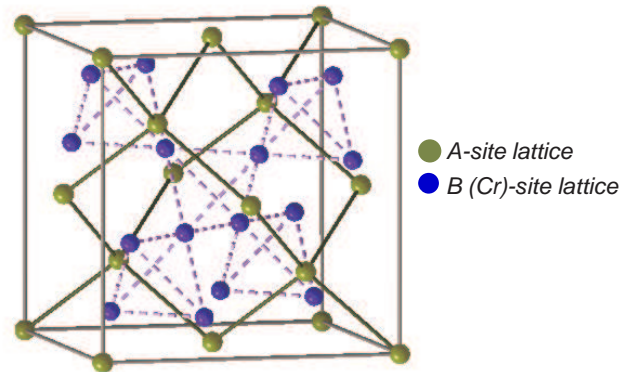


FIG. 1: Illustration of A and $B(\text{Cr})$ sublattices in the cubic unit cell of normal spinels $A\text{B}_2\text{X}_4$. The tetrahedrally coordinated Cr-atoms form a pyrochlore lattice.

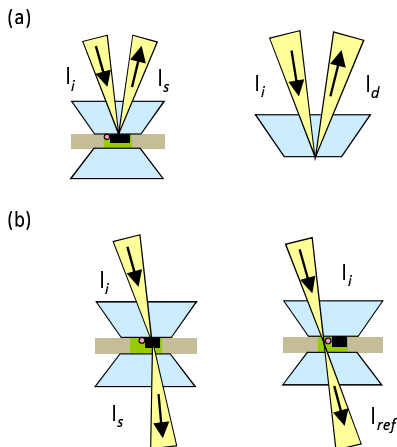


FIG. 2: Measurement configurations: (a) reflectance of a sample at the sample-diamond interface in a DAC and (b) transmittance of a sample in a DAC.

infrared reflection and transmission measurements under pressure in the frequency range 200-24000 cm^{-1} . The single crystals of ZnCr_2Se_4 and HgCr_2S_4 were grown by a chemical transport reactions,^{1,16} and CdCr_2O_4 was grown by a flux method.

The pressure-dependent reflectivity and transmission measurements were performed at room temperature, using a Bruker IFS 66v/S FTIR spectrometer. Far-infrared (FIR) reflectivity measurements were carried out at beamline IR1 of ANKA. The higher frequency measurements were carried out with conventional infrared radiation sources. A Syassen-Holzapfel diamond anvil cell (DAC),¹⁷ equipped with type IIa diamonds suitable for infrared measurements, was used to generate pressures up to 20 GPa.

A Bruker IR ScopeII infrared microscope with a 15 \times magnification objective coupled to the spectrometer was used to focus the infrared beam onto the small sample in the pressure cell. The samples were mechanically polished down to a thickness of $\approx 50 \mu\text{m}$ and a small piece of sample (about $80 \mu\text{m} \times 80 \mu\text{m}$ in size) was cut and loaded, together with CsI powder as pressure medium, in a $150 \mu\text{m}$ diameter hole drilled in a stainless steel gasket. Great care was taken when loading the sample, in order to obtain a clean and flat diamond-sample interface. With this crystal size and the corresponding diffraction limit, we were able to measure reliably in the frequency range down to 200 cm^{-1} . The ruby luminescence method¹⁸ was used for *in-situ* pressure determination. Variations in synchrotron source intensity were taken into account by applying additional normalization procedures.

The measurement geometries are shown in Fig. 2. In case of reflectivity measurements, spectra taken at the inner diamond-air interface of the empty cell served as the reference for normalization of the sample spectra. The absolute reflectivity at the sample-diamond in-

terface, denoted as R_{s-d} , was calculated according to $R_{s-d}(\omega) = R_{dia} \times I_s(\omega) / I_d(\omega)$, where $I_s(\omega)$ denotes the intensity spectrum reflected from the sample-diamond interface and $I_d(\omega)$ the reference spectrum of the diamond-air interface. $R_{dia} = 0.167$ was calculated from the refractive index of diamond n_{dia} . For obtaining the transmittance spectrum, the intensity transmitted through the sample I_s was divided by the intensity transmitted through the pressure transmitting medium I_{ref} i.e, $T(\omega) = I_s(\omega) / I_{ref}(\omega)$. The absorbance spectrum was calculated according to $A(\omega) = -\log_{10} T(\omega)$.

III. RESULTS

Reflectivity (R_{s-d}) spectra of ZnCr_2Se_4 , HgCr_2S_4 and CdCr_2O_4 are shown for few selected pressures in Fig. 3 (a), (b) and (c) in the frequency range 250-24000 cm^{-1} . The same curves are plotted separately in the low-frequency range [see Fig. 3 (d)-(f)] to better highlight the effect of pressure on the phonon modes. The region around 2000 cm^{-1} is cut out from the experimental spectra, due to strong diamond multi-phonon absorptions that cause artifacts in this spectral range. A linear interpolation has been performed in this range in order to perform the analysis.

For the analysis of the reflectivity data, we applied the Lorentz model, where the complex dielectric function is defined as:¹⁹

$$\epsilon(\omega) = \epsilon_\infty + \sum_j \frac{\Delta\epsilon_j \omega_{TOj}^2}{\omega_{TOj}^2 - \omega^2 + i\omega\gamma_j}, \quad (1)$$

In this model each mode is characterized by three parameters: the oscillator strength $\Delta\epsilon_j$, the frequency of transverse optical modes ω_{TOj} , and the damping of the modes γ_j . The fits along with the measured reflectivity spectra are shown in Fig. 3 as red dashed lines. The pressure dependence of the high-frequency permittivity ϵ_∞ used in our fitting was calculated according to the Clausius-Mossotti relation assuming ionic bonding:²⁰ $\frac{\epsilon_\infty(P)-1}{\epsilon_\infty(P)+2} = \frac{\tilde{\alpha}N}{3\epsilon_0V(P)}$, where $\tilde{\alpha}$ is the average atomic polarizability of the unit cell, obtained from the lowest-pressure data. $V(P)$ is the unit cell volume as a function of pressure calculated from the second-order Birch equation of state:^{21,22} $P(x) = \frac{3}{2}B_0x^{-7}(1-x^2)$, where $x = [\frac{V(P)}{V(0)}]^{1/3}$. The value of the bulk modulus was assumed to be $B_0=100$ GPa for ZnCr_2Se_4 and HgCr_2S_4 , and $B_0=200$ GPa for CdCr_2O_4 based on x-ray diffraction data.³ The obtained fit values were used for the extrapolation of the experimental reflectivity spectra to lower and higher frequencies necessary for the Kramers Kronig (KK) analysis.^{23,24} Since in case of HgCr_2S_4 the reflectivity data are noisy below 1000 cm^{-1} , the fit was used to obtain the real part of the optical conductivity.

To examine the electronic excitations in the chalcogenide compounds, the real part of the optical conductivity was considered (see Fig. 4). The optical conductivity

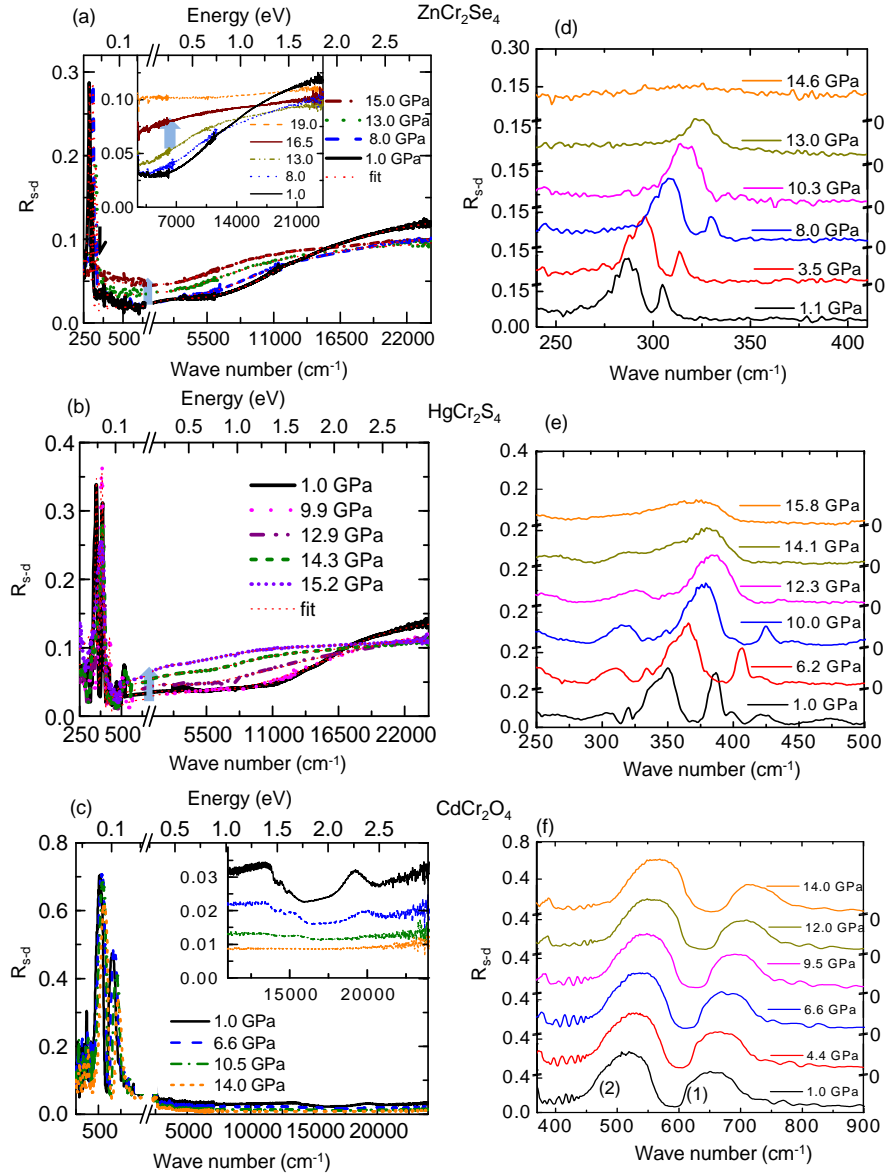


FIG. 3: Room-temperature reflectivity R_{s-d} spectra of (a) ZnCr_2Se_4 , (b) HgCr_2S_4 , and (c) CdCr_2O_4 in the spectral range $250\text{-}24000\text{ cm}^{-1}$ for selected pressures. The red dashed lines are fits with the Lorentz model. In (a) the small feature at around 400 cm^{-1} , marked with black arrow, is an artifact and not included in the fitting. Inset: Several selected R_{s-d} spectra in the pressure range $1\text{-}19.0\text{ GPa}$. In (c) the inset presents the magnification of the spectra in the frequency range $11000\text{-}24000\text{ cm}^{-1}$ to illustrate the very weak electronic excitations. The observed phonon modes of ZnCr_2Se_4 , HgCr_2S_4 and CdCr_2O_4 are presented in (d), (e) and (f), respectively. The spectra are offset for clarity. The screening of the phonon modes occur for ZnCr_2Se_4 , and HgCr_2S_4 with increasing pressure, while in case of CdCr_2O_4 the phonons remain intense up to the highest measured pressure.

spectra for ZnCr_2Se_4 and HgCr_2S_4 at the lowest pressure reveal an insulating behavior, with two phonon modes in the low-frequency range (which are not shown in Fig. 4) and a strong absorption band at about 15000 cm^{-1} and 15800 cm^{-1} , for ZnCr_2Se_4 and HgCr_2S_4 respectively. Upon pressure increase these bands broaden and gradually shift towards lower frequencies.

For CdCr_2O_4 the reflectivity above $\sim 5000\text{ cm}^{-1}$ is very low and exhibits only small changes under pressure [see

Fig. 3 (c)]. Therefore, additional transmission measurements were carried out on a single crystal of CdCr_2O_4 in the frequency range $8000\text{-}25000\text{ cm}^{-1}$ up to 20.2 GPa , especially in order to follow the effect of pressure on the high-frequency excitations. In Fig. 5 the transmittance and absorbance spectra of CdCr_2O_4 are depicted for selected pressures. These spectra show a pronounced absorption band at around 16760 cm^{-1} and weak features at 14500 cm^{-1} . The high-frequency contributions to the

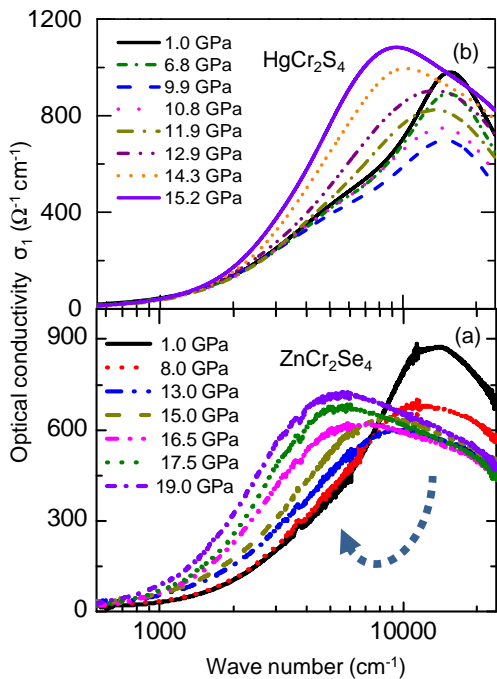


FIG. 4: Real part of the optical conductivity of (a) ZnCr_2Se_4 and (b) HgCr_2S_4 for selected pressures. The arrow indicates the red shift of the $d-d$ -transition ($10 Dq$).

absorbance spectra are shown in Fig. 6 for four selected pressures. The strong absorption band in CdCr_2O_4 exhibits a blue shift under pressure (see below for a quantitative analysis of the spectra).

In all three compounds a strong absorption bands is observed at energies (see Table I) which are very close to the ones which have been attributed to spin-allowed intra-atomic $d-d$ excitations (crystal-field excitations):^{10,25–31} The Cr^{3+} ion in an octahedral environment exhibits two spin-allowed crystal-field (CF) transitions, namely from the ${}^4A_{2g}$ ground state to the ${}^4T_{2g}$ and ${}^4T_{1g}$ excited states. The transition from the ground state to ${}^4T_{2g}$ is located at $10 Dq$ (Δ_{oct}), where Dq is the Coulombic parameter of the ligand field. Usually, the CF-transitions are parity-forbidden because of the inversion symmetry at the transition-metal ion site. These transitions can become allowed by virtue of lattice vibrations, which locally break the center of symmetry.^{10,26,29} This interpretation is certainly fulfilled in the case of the oxide CdCr_2O_4 ,

Compounds	Frequency
CdCr_2O_4	16760 cm^{-1}
HgCr_2S_4	15800 cm^{-1}
ZnCr_2Se_4	15000 cm^{-1}

TABLE I: The energies of the electronic transitions for the three investigated Cr-spinel compounds at ~ 1 GPa.

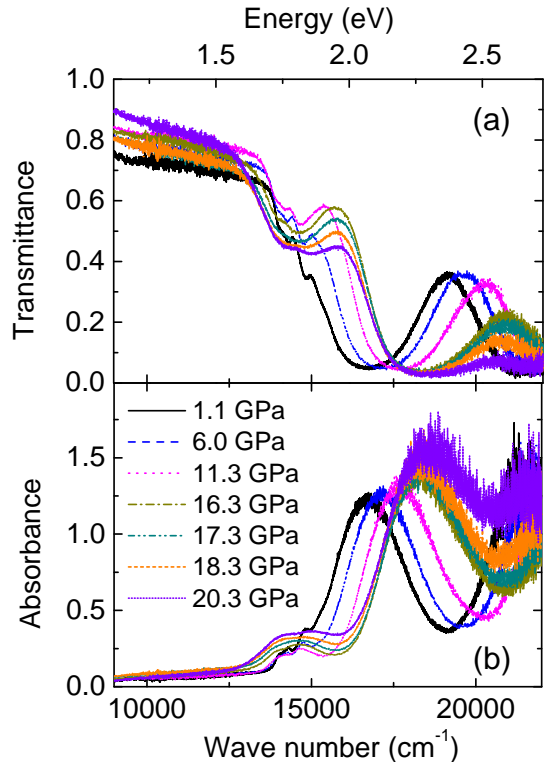


FIG. 5: (a) Transmittance and (b) absorbance spectra of CdCr_2O_4 for several selected pressures.

where these excitations can only be observed in transmission. With increasing pressure the CF-splitting is expected to increase resulting in a blue shift of the CF excitations,^{32,33} in agreement with our findings.

The rather large oscillator strength of the corresponding electronic excitations in the chalcogenides can only be understood if strong hybridization effects between the chalcogenide p -states and the chromium d -states occur, and an interpretation of pure CF transition is not adequate anymore.³⁴ The mixed character of the electronic states for the chalcogenide may also explain the observed red shift under pressure in contrast to the blue shift observed for the oxide.

In Ref.28 the center of gravity of CF excitations for many chromium complexes are given, where Cr^{3+} is in octahedral environment. The energies of two spin-allowed transitions from the ground state ${}^4A_{2g}$ to the excited levels ${}^4T_{2g}$ and ${}^4T_{1g}$ vary from ≈ 13000 - 17000 cm^{-1} and ≈ 17000 - 22000 cm^{-1} , respectively. The spin-forbidden transitions ${}^4A_{2g}$ to 2E_g and ${}^2T_{2g}$ vary from 13000 - 14400 cm^{-1} and 18000 - 19200 cm^{-1} , respectively.

Indeed, for CdCr_2O_4 weak features (marked by arrows) are observed at around 14500 cm^{-1} in addition to the strong absorption band. They are attributed to spin-forbidden transitions, which become allowed due to spin-orbit coupling.³² At low temperature six spin-forbidden transitions can be found, which broaden with increas-

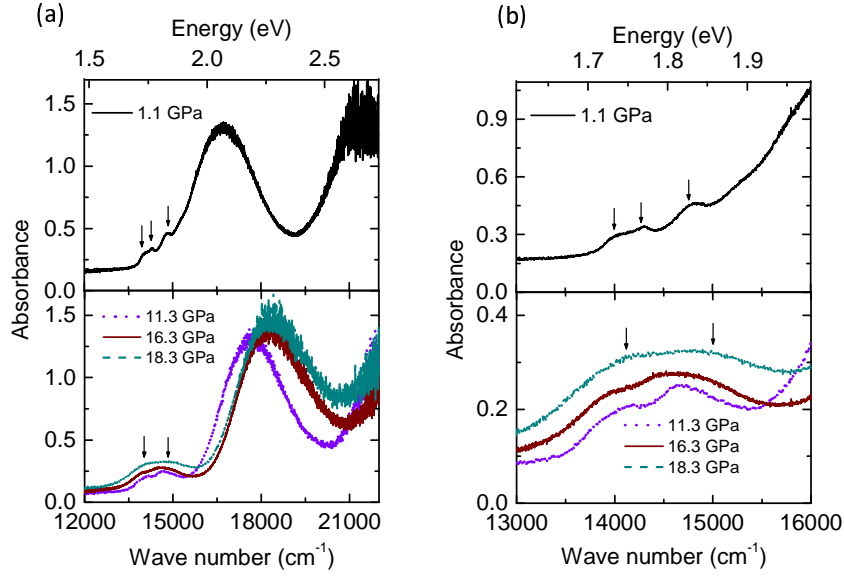


FIG. 6: (a) Absorbance spectrum of CdCr₂O₄ at 1.1 GPa shows four features: one strong feature at ≈ 16760 cm⁻¹, and three weak features marked with black arrows. At higher pressures (11.3, 16.3 and 18.3 GPa) only two low-energy absorption features marked with black arrows are resolvable. (b) Low-energy part of the spectra to illustrate the pressure dependence of the spin-forbidden transitions (marked with arrows).

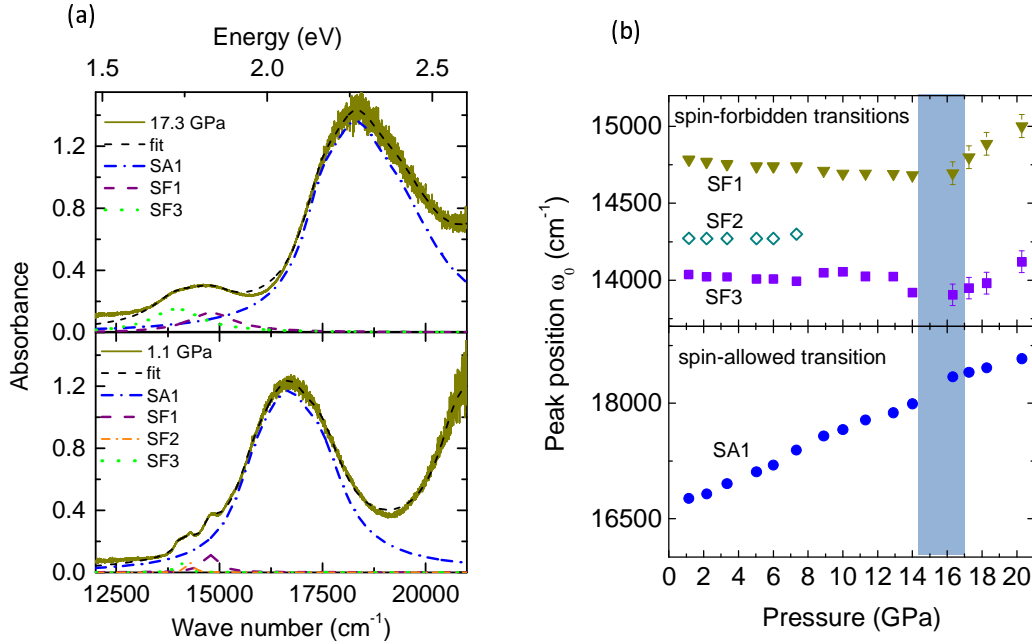


FIG. 7: (a) Fit of the absorption spectrum of CdCr₂O₄ at 1.1 GPa and 17.3 GPa consisting of four and three absorption features, respectively. (b) Peak position ω_0 of the absorption features as a function of pressure. The shaded area marks the transition region.

ing temperature and can not be completely resolved anymore at room temperature,²⁹ consistent with our data. We used Lorentz oscillators to describe the spin-allowed and spin-forbidden transitions at room temperature. The strong absorption band at $\omega_0 \approx 16760$ cm⁻¹ (SA1) shows a

blue shift with increasing pressure, as shown in Fig. 7 (b), but there is no significant frequency shift of the spin-forbidden excitations (SF1, SF2, SF3) up to 8 GPa. Above 8 GPa the three transitions are not distinguishable anymore, and the curves are fitted with two over-damped

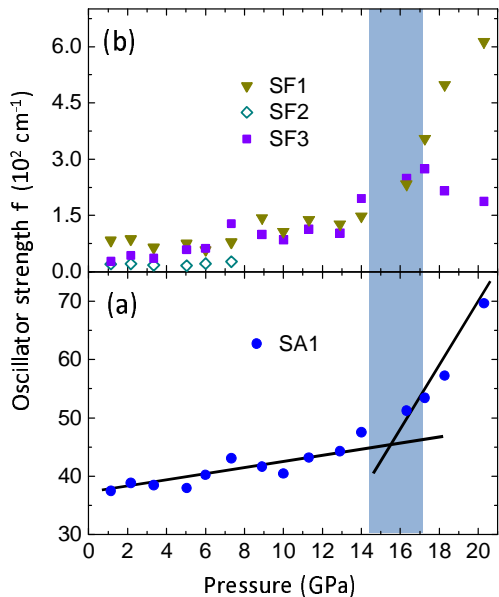


FIG. 8: Oscillator strength of the observed $d-d$ -transitions of CdCr_2O_4 . (a) Oscillator strength of the spin-allowed transition (SA1) increases with increasing pressure. (b) Oscillator strength of the spin-forbidden transitions (SF1, SF2, SF3), which is very small compared to the total oscillator strength. The shaded area marks the transition region and the black solid lines are guides to the eye.

absorption bands. An anomalous change in their central frequencies can be seen at 14 GPa [see Fig.7 (b)], showing a blue shift on further pressure increase.

The oscillator strength of the excitations was calculated according to

$$f = \int_{\omega_1}^{\omega_2} A(\omega) d\omega, \quad (2)$$

with the absorbance $A(\omega)$, $\omega_1=9000 \text{ cm}^{-1}$, and $\omega_2=22000 \text{ cm}^{-1}$. The oscillator strength of the spin-allowed transition increases with increasing pressure [see Fig. 8(a)]. Above $P_c \approx 16 \text{ GPa}$ the pressure-induced increase in oscillator strength is drastically enhanced. The three spin-forbidden transitions contribute very little to the total oscillator strength, but overall the oscillator strength of these features increases with pressure up to $\approx 15 \text{ GPa}$; at this pressure anomalies occur [see Fig. 8(b)].

In the far-infrared region we resolve two phonon modes [mode (1) and (2)] out of four predicted modes, since the other two low-frequency phonon modes are beyond the studied frequency range. For a more detailed discussion of the phonon modes and their evolution with pressure we refer to section IV. To extract the frequency, oscillator strength, and damping of the modes, the low-frequency reflectivity spectra were fitted with the Lorentz model. The illustration of the fit for three selected pressures for each compound and the so-obtained results for the fitting parameters are shown in Fig. 9.

For ZnCr_2Se_4 [see Fig. 9 (d)] the phonon modes harden with increasing pressure. There is no significant change in damping and oscillator strength of both phonon modes up to $P \approx 10 \text{ GPa}$. Above this pressure phonon mode (1) is no longer visible. By further increasing the pressure, the remaining mode (2) starts to lose its strength and broadens. At 14 GPa the phonon resonances can no longer be clearly resolved.

In the case of HgCr_2S_4 , the two phonon modes harden with increasing pressure up to 12 GPa. Above 12 GPa the mode (1) is no longer visible and the mode (2) softens with increasing pressure. There is no significant change in oscillator strength of mode (1), but it starts to become more damped at around 8 GPa as shown in Fig. 9 (e). With further increasing pressure the damping increases and the mode (1) can no longer be resolved above 12 GPa. Mode (2) behaves differently, since there is no significant change in the damping up to 11 GPa. By further increasing the pressure the damping increases and also the oscillator strength of mode (2) increases. The phonon parameters show an anomaly at around 12 GPa [see Fig. 9 (e)].

In CdCr_2O_4 the phonon modes harden with increasing pressure and there is no notable change in the oscillator strength of both modes (1) and (2) up to the highest measured pressure ($P \approx 14 \text{ GPa}$) [see Fig. 9 (f)]. Mode (1) loses intensity upon pressure application, but mode (2) shows only small modifications up to the highest measured pressure.

IV. DISCUSSION

The optical properties of Cr-spinels have been extensively studied by various experimental methods. In literature there are numerous Raman and infrared studies reporting about the phonon frequencies for various pure and mixed spinels. From the lattice symmetry of the normal spinels, the group theory analysis predicts four infrared-active triply degenerate T_{1u} phonon modes in the FIR spectrum:³⁵

$$\begin{aligned} \Gamma &= 4T_{1u} && (IR - active) \\ &+ A_{1g} + E_{1g} + 3T_{2g} && (Raman - active) \\ &+ 2A_{2u} + 2E_u + T_{1g} + 2T_{2u} && (Silent) \end{aligned}$$

We have chosen to label the four IR-active modes as (1) to (4), starting from high to low frequencies. The origin of the T_{1u} modes has been the subject of controversy as two possible interpretations were proposed: In one case the two high-frequency phonon modes are related to the displacement of the Cr-X bond in the CrX_6 octahedra, while the two low-frequency phonon modes to the tetrahedra.^{16,36,37} It has been shown experimentally³⁸⁻⁴⁰ that the materials having an octahedral sublattice as one of the structural units exhibit phonon modes belonging to octahedral vibrations at higher-frequencies compared to the other lattice vibrations.

On the other hand, Lutz and coworkers⁴¹⁻⁴⁶ claimed

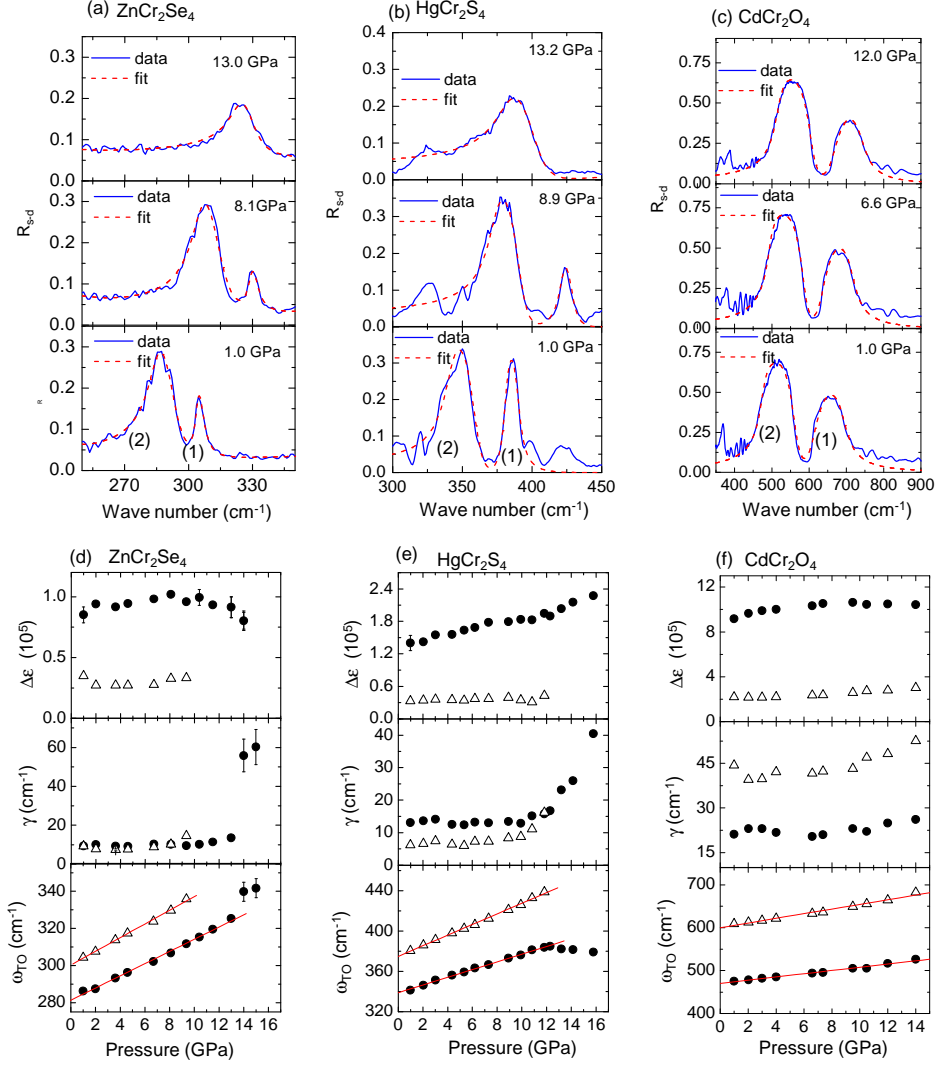


FIG. 9: Illustration of the fit of two observed phonon modes named as (1) and (2) with the Lorentz model according to Eq. 1 for selected pressures for (a) ZnCr_2Se_4 , (b) HgCr_2S_4 , and (c) CdCr_2O_4 . The obtained results from the fit are shown below of each relative compound (see d-f). The pressure-dependence of frequencies of optical phonons are fitted according to Eq. 3 to find the initial linear pressure coefficient.

that almost all atoms contribute to the four IR-active phonon modes. They proposed that the contribution of A -site atoms to the higher-frequency phonon modes (mode (1) and (2)) is smaller compared to that to the two lower-frequency phonon modes. An assignment of the phonon modes to vibrations of tetrahedral AX_4 , octahedral BX_6 or cubic B_4X_4 units of the structure is, within this framework, not possible.⁴² However, one can hypothesize that for higher-frequency phonon modes the contribution of octahedral vibrations is larger compared to that of tetrahedral vibrations.

It has been predicted theoretically that in normal spinels the octahedral BX_6 unit is much more ionic than the tetrahedral AX_4 , and the value of the force constant for Cr-X is larger than that of $A-X$.^{43,44} In infrared experiments the oscillator strength is directly related to the

ionicity of a bond.⁴⁷ The more ionic the character of the bond is, the stronger will be the vibrational mode belonging to that bond. The mode (2) is stronger compared to mode (1), indicating a larger contribution of BX_6 octahedra [see Fig. 9 (d)-(f)]. Furthermore, the mode intensities decrease moving from the oxide over the sulfide to the selenides, which suggests an increasing covalency of the bonds.¹

With increasing pressure all phonon modes shift to higher frequencies in a linear fashion [see Fig. 9 (d)-(f)]. The linear pressure coefficient, C , in the low-pressure regime was obtained by fitting the frequency of the phonon modes with the following equation:

$$\omega(P) = \omega_o + C \times P, \quad (3)$$

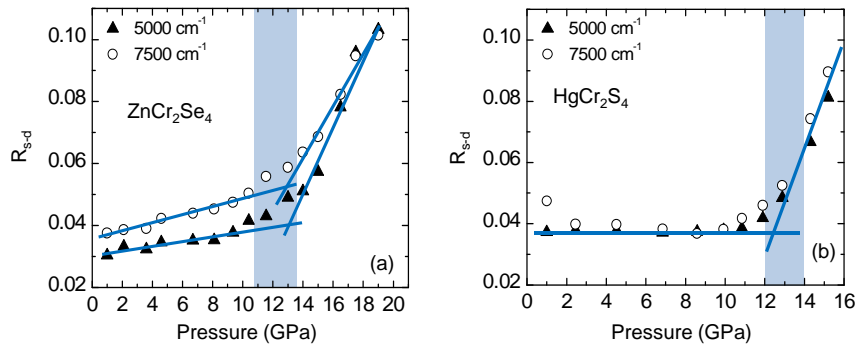


FIG. 10: Estimation of P_c for (a) ZnCr_2Se_4 and (b) HgCr_2S_4 by plotting the change in reflectivity R_{s-d} level with increasing pressure at 5000 cm^{-1} and 7500 cm^{-1} shown with solid triangles and open circles, respectively. The shaded areas mark the transition region and the full lines are guides to the eye.

where P is the applied pressure, ω_o is the phonon frequency at zero pressure and C is the linear pressure coefficient. The obtained results are given in Table II. The value of C represents the stiffness of bonds, and therefore can serve as a measure for the compressibility of the compound. In all investigated Cr-spinel compounds, the value of C for mode (2) is smaller compared to mode (1), which attributes to the fact that the respective bonding of mode (2) is stiffer compared to mode (1). Moreover the C values for the phonon modes of CdCr_2O_4 and HgCr_2S_4 are larger than that of ZnCr_2Se_4 .

Regarding the compressibility difference for the three investigated compounds, the foremost consideration is the part of the unit cell volume, which is mainly occupied by anions. The compressibility is mainly determined by the X-sublattice,^{3,15} since the number of X-X bonds is larger compared to the other bonds (i.e., Cr-X and A-X bonds). In the periodic table, the electronegativity decreases from oxygen to selenium, while the size of ions increases. The selenium (Se^{2-}) ion is bigger as compared to sulphur (S^{2-}) and oxygen (O^{2-}) and this corresponds to a larger bond length of chalcogenides compared to oxides. Application of external pressure will affect the longer bond length stronger than the shorter bond length. With these considerations, the chalcogenides are expected to be more compressible as compared to the oxides. The higher compressibility corresponds to a more covalent character of the chemical bond and a lower ionicity of the anions.³ ZnCr_2Se_4 shows semiconducting char-

acter, while CdCr_2O_4 shows insulating behavior as covalency increases from the oxide to the selenide. In this respect, the rather small values of the linear pressure coefficient C for the modes in ZnCr_2Se_4 are surprising.

For the investigated chalcogenide compounds the phonon parameters exhibit anomalies in their pressure dependence: For ZnCr_2Se_4 anomalies occur at $P_c \approx 10$ GPa, which are interpreted in terms of a structural phase transition from cubic to tetragonal symmetry. This is supported by an X-ray powder diffraction study³ where a pressure-induced structural phase transformation from cubic ($\text{Fd}\bar{3}\text{m}$) to tetragonal ($\text{I}\bar{4}$) was reported for CdCr_2Se_4 at around 10 GPa. The phonon parameters of HgCr_2S_4 show an anomaly at around 12 GPa, which is supported by a very recent Raman study of HgCr_2S_4 under pressure. A splitting of vibrational Raman modes was observed starting at around 12 GPa and related to a structural phase transition from a cubic to a tetragonal symmetry observed by diffraction methods.⁴⁸ The compressibility of oxides is low compared to the chalcogenides, since the chemical bonds are very stiff, and therefore the critical pressure is expected to be higher. Indeed, a Raman study of ZnCr_2O_4 under pressure reveals a sluggish structural phase transition starting at 17.5 GPa, which is completed at around 35 GPa.⁴⁹ Consistent with this is the absence of an anomaly for the phonon modes in CdCr_2O_4 up to 14.0 GPa according to our data.

Signatures of the pressure-induced structural phase transition are also expected in the pressure evolution of the electronic excitations. Therefore, we plot in Fig. 10 the change in the reflectivity spectra as a function of pressure at 5000 cm^{-1} and 7500 cm^{-1} for ZnCr_2Se_4 and HgCr_2S_4 , since the reflectivity in this range relates to the electronic excitations in the materials. For ZnCr_2Se_4 the reflectivity versus pressure curve shows a continuous increase in R_{s-d} with increasing pressure up to 10 GPa. By further increasing pressure there is drastic increase in R_{s-d} indicating that the new structural phase is more

Compounds	Phonon mode (1)	Phonon mode (2)
CdCr_2O_4	5.41 ± 0.25	3.75 ± 0.17
HgCr_2S_4	5.25 ± 0.08	3.80 ± 0.06
ZnCr_2Se_4	3.68 ± 0.10	3.28 ± 0.07

TABLE II: Values of the linear pressure coefficient C ($\text{cm}^{-1}/\text{GPa}$) for two phonon modes of the three investigated Cr-spinel compounds.

susceptible to external pressure. In case of HgCr_2S_4 there is a drastic increase in R_{s-d} above 12 GPa; below this pressure the reflectivity level remains almost constant at selected frequencies [see Fig. 10(b)]. CdCr_2O_4 shows an anomaly in the oscillator strength of the CF excitations at $P_c \approx 15$ GPa [see Figs. 7(b) and 8]. A higher value of the critical pressure for CdCr_2O_4 as compared to the chalcogenides is consistent with our low-frequency results.

V. SUMMARY

The Cr-spinel compounds ZnCr_2Se_4 , HgCr_2S_4 , and CdCr_2O_4 were studied by optical spectroscopy under pressure. With increasing pressure all observed phonon modes shift linearly to higher frequencies in the low-pressure regime. For ZnCr_2Se_4 and HgCr_2S_4 the elec-

tronic excitations exhibit a red shift upon pressure application, whereas for CdCr_2O_4 they show a blue shift. According to the anomalies found in the phonon behavior, reflectivity level, and the electronic excitations all three compounds undergo a pressure-induced structural phase transition with the critical pressure $P_c \approx 10, 12, 15$ GPa for ZnCr_2Se_4 , HgCr_2S_4 , and CdCr_2O_4 , respectively.

Acknowledgements

We acknowledge the ANKA Angströmquelle Karlsruhe for the provision of beamtime and thank B. Gasharova, Y.-L. Mathis, D. Moss, and M. Süpfle for assistance using the beamline ANKA-IR. Financial support by the Bayerische Forschungsstiftung and the DFG (Emmy Noether-program, SFB 484, TRR 80) is acknowledged.

-
- * E-mail: christine.kuntscher@physik.uni-augsburg.de
- ¹ T. Rudolf, Ch. Kant, F. Mayr, J. Hemberger, V. Tsurkan, and A. Loidl, *New J. Phys.* **9**, 76 (2007).
 - ² S.-H. Lee, C. Broholm, W. Ratcliff, G. Gasparovic, Q. Huang, T. H. Kim, and S.-W. Cheong, *Nature* **418**, 856 (2002).
 - ³ A. Waškowska, L. Gerward, J. Staun Olsen, and E. Malicka, *J. Phys.: Condens. Matter* **14**, 12423 (2002).
 - ⁴ J. Hemberger, P. Lunkenheimer, R. Ficht, H.-A. Krug von Nidda, V. Tsurkan, and A. Loidl, *Nature* **434**, 364 (2005).
 - ⁵ G. Xu, H. Weng, Z. Wang, X. Dai, and Z. Fang, *Phys. Rev. Lett.* **107**, 186806 (2011).
 - ⁶ Y. Yamashita and K. Ueda, *Phys. Rev. Lett.* **85**, 4960 (2000).
 - ⁷ O. Tchernyshyov, R. Moessner, and S. L. Sondhi, *Phys. Rev. Lett.* **88**, 067203 (2002).
 - ⁸ T. Watanabe, *J. Phys. Soc. Jpn.* **37**, 140 (1974).
 - ⁹ Ch. Kant, J. Deisenhofer, T. Rudolf, F. Mayr, F. Schrettle, A. Loidl, V. Gnezdilov, D. Wulferding, P. Lemmens, and V. Tsurkan, *Phys. Rev. B* **80**, 214417 (2009).
 - ¹⁰ T. Rudolf, Ch. Kant, F. Mayr, M. Schmidt, V. Tsurkan, J. Deisenhofer, and A. Loidl, *Eur. Phys. J. B* **68**, 153 (2009).
 - ¹¹ R. V. Aguilar, A. B. Sushkov, Y. J. Choi, S.-W. Cheong, and H. D. Drew, *Phys. Rev. B* **77**, 092412 (2008).
 - ¹² S. Massidda, M. Posternak, A. Baldereschi, and R. Resta, *Phys. Rev. Lett.* **82**, 430 (1999).
 - ¹³ Ch. Kant, M. Schmidt, Zhe Wang, F. Mayr, V. Tsurkan, J. Deisenhofer, and A. Loidl, *Phys. Rev. Lett.* **108**, 177203 (2012).
 - ¹⁴ H. D. Lutz, G. Wäschenbach, G. Kliche, and H. Haeuseler, *J. Solid State Chem.* **48**, 196 (1983).
 - ¹⁵ A. Waškowska, L. Gerward, J. Staun Olsen, M. Feliz, R. Llusar, L. Gracia, M. Marqués, and J. M. Recio, *J. Phys.: Condens. Matter* **16**, 53 (2004).
 - ¹⁶ T. Rudolf, Ch. Kant, F. Mayr, J. Hemberger, V. Tsurkan, and A. Loidl, *Phys. Rev. B* **75**, 052410 (2007).
 - ¹⁷ G. Huber, K. Syassen, and W. B. Holzapfel, *Phys. Rev. B* **15**, 5123 (1977).
 - ¹⁸ H. K. Mao, J. Xu, and P. M. Bell, *J. Geophys. Res., [Atmos]* **91**, 4673 (1986).
 - ¹⁹ F. Gervais, *in Infrared and Millimeter Waves*, edited by K. J. Button, Academic, New York, USA (1983).
 - ²⁰ N. W. Ashcroft and N. D. Mermin, *Solid State Physics* (Harcourt Brace College Publishers), (1976).
 - ²¹ F. Birch, *J. Geophys. Res.* **83**, 1257 (1978).
 - ²² W. B. Holzapfel, *Rep. Prog. Phys.* **59**, 29 (1996).
 - ²³ J. S. Plaskett and P. N. Schatz, *J. Chem. Phys.* **38**, 612 (1963).
 - ²⁴ A. Pashkin, M. Dressel, and C. A. Kuntscher, *Phys. Rev. B* **74**, 165118 (2006).
 - ²⁵ A. D. Liehr, *J. Phys. Chem.* **67**, 1314 (1963).
 - ²⁶ B. N. Figgis and M. A. Hitchman, *Ligand Field Theory and its Applications*, Wiley-VCH, New York (1999).
 - ²⁷ K. Ohgushi, Y. Okimoto, T. Ogasawara, S. Miyasaka, and Y. Tokura, *J. Phys. Soc. Jpn.* **77**, 034713 (2008).
 - ²⁸ C. K. Jorgensen, *Inorg. Chem. Acta Rev.* **2**, 65 (1968).
 - ²⁹ M. Schmidt, Zhe Wang, Ch. Kant, F. Mayr, S. Toth, A. T. M. N. Islam, B. Lake, V. Tsurkan, A. Loidl, and J. Deisenhofer, *Phys. Rev. B* **87**, 224424 (2013).
 - ³⁰ P. K. Larsen and S. Wittekoek, *Phys. Rev. Lett.* **29**, 1597 (1972).
 - ³¹ L. L. Golik, Z. É. Kunkova, T. G. Aminov, and G. G. Shabunina, *Phys. Solid State* **38**, 717 (1996).
 - ³² S. Sugano, Y. Tanabe, and H. Kamimura, *Multiplets of transition-metal ions in crystals*, Academic Press, New York and London., (1970).
 - ³³ C. A. Kuntscher, A. Pashkin, H. Hoffmann, S. Frank, M. Klemm, S. Horn, A. Schönleber, S. van Smaalen, M. Hanfland, S. Glawion, M. Sing, and R. Claessen, *Phys. Rev. B* **78**, 035106 (2008).
 - ³⁴ M. Taniguchi, A. Fujimori, and S. Suga, *Solid State Commun.* **70**, 191 (1989).
 - ³⁵ K. Wakamura, T. Arai, and K. Kudo, *J. Phys. Soc. Jpn.* **40**, 1118 (1976).
 - ³⁶ D. Basak and J. Ghose, *Spectrochimica. Acta.* **50A**, 713 (1994).
 - ³⁷ C. J. Fennie and K. M. Rabe, *Phys. Rev. B* **72**, 214123 (2005).
 - ³⁸ K. Thirunavukkuarasu, F. Lichtenberg, and C. A. Kuntscher, *J. Phys.: Condens. Matter* **18**, 9173 (2006).

- ³⁹ R. Haumont, P. Bouvier, A. Pashkin, K. Rabia, S. Frank, B. Dkhil, W. A. Crichton, C. A. Kuntscher, and J. Kreisel, *Phys. Rev. B* **79**, 184110 (2009).
- ⁴⁰ J. Preudhomme and P. Tarte, *Spectrochimica. Acta.* **27A**, 1817 (1971).
- ⁴¹ H. D. Lutz and H. Haeuseler, *J. Mol. Struct.* **511-512**, 69 (1999).
- ⁴² H. D. Lutz, J. Himmrich, and J. Haeuseler, *Z. Naturforsch.* **45a**, 893 (1990).
- ⁴³ J. Zwinscher and H. D. Lutz, *J. Solid State Chem.* **118**, 43 (1995).
- ⁴⁴ J. Zwinscher and H. D. Lutz, *J. Alloys Compd.* **219**, 103 (1995).
- ⁴⁵ C. Kringe, B. Oft, V. Schellenschläger, and H. D. Lutz, *J. Mol. Struct.* **596**, 25 (2001).
- ⁴⁶ J. Himmrich and H. D. Lutz, *J. Solid State Commun.* **79**, 447 (1991).
- ⁴⁷ K. Wakamura and T. Arai, *Phase Transitions* **27**, 129 (1990).
- ⁴⁸ Ilias Efthimiopoulos, Alexander Yaresko, Vladimir Tsurkan, Joachim Deisenhofer, Alois Loidl, Changyong Park, and Yuejian Wang, *Appl. Phys. Lett.* **103**, 201908 (2013).
- ⁴⁹ Z. Wang, P. Lazor and G. Artioli, *J. Solid State Chem.* **165**, 165 (2002).